Article

Not peer-reviewed version

Nanostructured Electrospun Fibers with Self-assembled Cyclo-L-Tryptophan-L-Tyrosine Dipeptide as Piezoelectric Materials and Optical Second Harmonic Generators

Daniela Santos , Rosa M. F. Baptista * , Adelino Handa , Bernardo Almeida , Pedro V. Rodrigues , Cidália Castro , Ana Machado * , Manuel J. L. F. Rodrigues , Michael Belsley , Etelvina De Matos Gomes

Posted Date: 21 June 2023

doi: 10.20944/preprints202306.1571.v1

Keywords: cyclo-dipeptide; electrospinning; piezoelectricity; nanofibers; optical second harmonic generation; self-assembly

Article

Nanostructured Electrospun Fibers with Self-assembled Cyclo-L-Tryptophan-L-Tyrosine Dipeptide as Piezoelectric Materials and Optical Second Harmonic Generators

Daniela Santos [1], Rosa M. F. Baptista [1,*], Adelino Handa [1], Bernardo Almeida [1], Pedro V. Rodrigues [2], Cidália Castro [2], Ana Machado [2,*], Manuel J. L. F. Rodrigues [1], Michael Belsley [1] and Etelvina de Matos Gomes [1]

[1] Laboratory for materials and Emergent Technologies (LAPMET), Centre of Physics of Minho and Porto Universities (CF-UM-UP), University of Minho, Campus de Gualtar, 4710-057 Braga, Portugal
[2] Institute for Polymers and Composites, University of Minho, Campus de Azurém, 4800-058 Guimarães, Portugal
* Correspondence: rosa_batista@fisica.uminho.pt and avm@dep.uminho.pt

Abstract: The potential use of nanostructured dipeptide self-assemblies in materials science for energy harvesting devices is a highly sought-after area of research. Specifically, aromatic cyclo-dipeptides containing tryptophan have garnered attention due to their wide-bandgap semiconductor properties, high mechanical rigidity, photoluminescence, and nonlinear optical behavior. In this study, we present the development of a hybrid system comprising biopolymer electrospun fibers incorporated with the chiral cyclo-dipeptide L-Tryptophan-L-Tyrosine. The resulting nanofibers are wide-bandgap semiconductors (bandgap energy 4.0 eV) and consist of self-assembled nanotubes embedded within a polymer matrix, exhibiting intense blue photoluminescence. Moreover, the cyclo-dipeptide L-Tryptophan-L-Tyrosine incorporated into polycaprolactone nanofibers displays a strong effective second harmonic generation signal of 0.36 pm/V and also shows notable piezoelectric properties with a high effective coefficient of 22 pCN^{-1}. These hybrid systems hold great promise for applications in the field of nanoenergy harvesting and nanophotonics.

Keywords: cyclo-dipeptide; electrospinning; piezoelectricity; nanofibers; optical second harmonic generation; self-assembly

1. Introduction

Bionanotechnology is an emerging area with the potential to revolutionize various fields of science and technology. By combining the principles of biology and nanotechnology, researchers are developing new ways to design and manipulate biological systems at the nanoscale level.

The impact of nanotechnology has been substantial across industries and society as a whole. In the medical field, for instance, bionanotechnology is driving the development of advanced imaging techniques, targeted drug delivery systems, customized medical devices and therapeutics for specific diseases [1]. Similarly, in energy production, bionanotechnology is being used to develop more efficient and sustainable methods of energy generation and storage [2]. Moreover, in environmental science, bionanotechnology facilitates the creation of novel materials and sensors capable of detecting and eliminating pollutants from the environment [3]. Consequently, bionanotechnology has the potential to drive innovation and create new solutions to the complex problems we face as a society.

One class of biomolecules that holds great promise in bionanotechnology is peptides. Peptides, consisting of short chains of amino acids, exhibit diverse structures, functions, and biological activities [4]. Among these, cyclic dipeptides or cyclo-dipeptides (CDPs) represent a noteworthy category. CDPs consist of two amino acids connected by a peptide bond, forming a ring structure. These cyclic 2,5-diketopiperazines offer enhanced bioactivity, structural rigidity, biofunctionalization and enzymatic stability [5,6].

 doi:10.20944/preprints202306.1571.v1

CDPs are known to exhibit a variety of biological activities, including antimicrobial and anticancer properties. Moreover, they possess the remarkable ability to undergo self-assembly processes, forming various nanostructures with distinct functions [7]. Through engineering, CDPs can be manipulated to self-assemble into nanoscale structures, such as nanotubes, nanofibers, nanowires, and nanospheres, displaying unique properties depending on their sequence and the surrounding environment [8,9].

Recent studies have revealed that aromatic groups found in organic materials, including dipeptide nanostructures, exhibit enhanced rigidity and possess stronger mechanical, optical, and piezoelectric properties upon self-assembly. This makes them highly promising candidates for a wide range of applications, including next-generation biocompatible energy harvesting nanogenerators, biosensors, and optical waveguides [10,11].

Self-assembly, a fundamental process in bionanotechnology, refers to the spontaneous organization of individual units, such as molecules or nanoparticles, into well-ordered structures or systems without external control [4]. This process occurs through non-covalent interactions, such as hydrogen bonding, electrostatic interactions, Van der Waals forces, $\pi - \pi$ and hydrophobic interactions [12]. These interactions play a crucial role in driving the self-assembly of organic materials, facilitating the formation of intricate nanostructures with tailored functionalities.

The mechanisms underlying self-assembly offer opportunities for designing and synthesizing new materials and devices with customized properties and functions. CDPs, in particular, hold great promise in bionanotechnology due to their biocompatibility, structural rigidity, flexibility in morphology, and ease of modification and preparation [5,12]. When combined with other nanomaterials and technologies, CDPs can be used to create novel materials and devices with unique functions and properties, applicable in a wide range of fields, including tissue engineering, drug delivery, biosensors, and diagnostic devices [6,8,9,13].

Notably, studies have shown that CDPs, especially those incorporating the amino acid tryptophan, can self-assemble through supramolecular phases involving hydrogen bonding and aromatic interactions (such as aromatic stacking or aromatic interlocks) [14]. This supramolecular assembly results in smaller bandgap energies, thereby improving conductivity and photoluminescence, and enhancing mechanical strength and piezoelectric properties [8,13,15].

The incorporation of cyclic dipeptides into polymer fibers is of significant relevance due to the potential conferred by employing a flexible and versatile polymeric matrix. These CDPs, characterized by their ring structure, contribute to structural rigidity, biofunctionalization, and improved mechanical properties [16]. Such polymer fibers with cyclic dipeptides offer the prospect of developing materials exhibiting superior mechanical characteristics, including heightened tensile strength and flexibility, rendering them well-suited for diverse technological applications, including composite materials, microelectronic device manufacturing, and tissue engineering. The amalgamation of a flexible and versatile polymeric matrix with cyclic dipeptides facilitates the creation of innovative materials endowed with enhanced mechanical and piezoelectric performance, thereby furnishing advanced and efficient solutions for a myriad of technological requirements.

Electrospinning is a technique used to produce fibers with diameters ranging from a few nanometers to several micrometers, and can be employed to create fibers incorporating the CDP L-tryptophan-L-tyrosine within the polymeric matrix. The process involves the use of electrostatic repulsive forces to draw a polymer solution into nanofibers extruded from the tip of the needle and collected in a grounded collector [17].

The nanofiber morphology can be controlled by varying the experimental parameters. As such, it is crucial to carefully select several factors that can influence the electrospinning process, including the properties of the polymer solution (concentration and viscosity), the flow rate of the solution, the electric field strength, the distance between the tip of the needle and the collector (TCD), and the environmental conditions such as temperature and humidity [18]. The properties of the polymer solution, such as its viscosity and

 doi:10.20944/preprints202306.1571.v1

conductivity, play a critical role in determining the final fiber diameter and morphology. A higher applied voltage or a smaller TCD can result in smaller fiber diameters, but can also lead to beading and uneven fiber distribution [17]. Environmental factors such as temperature and humidity can affect the properties of the polymer solution, leading to changes in the fiber morphology and diameter. Understanding the influencing factors of the electrospinning process is critical for controlling the fiber diameter and morphology and maximizing the performance of the resulting nanofibers in various applications.

The understanding and study of the second harmonic generation and piezoelectric properties in these hybrid systems incorporated with cyclic dipeptides are of utmost importance. These properties offer opportunities for the creation of advanced and innovative devices in various fields. Second harmonic generation is a nonlinear optical property that allows for the efficient conversion of a single light beam into two photons of higher energy [19–21]. This can be applied in energy generation devices and optical communication technologies. On the other hand, piezoelectricity is the ability of certain materials to generate an electric charge when subjected to mechanical stress, and vice versa [22]. This property is crucial in pressure sensors, mechanical energy devices, and energy conversion systems. Therefore, exploring and understanding these properties in the systems of fibers incorporated with cyclic dipeptides can lead to the development of new materials and devices with innovative functionalities, paving the way for advanced applications in areas such as energy, electronics and medicine.

2. Materials and Methods

2.1. Materials

The chiral cyclic dipeptide cyclo-L-tryptophan-L-tyrosine, hereafter referred as Cyclo(L-Trp-L-Tyr) (Mw = 349.39 g/mol), was purchased from Bachem AG (Bubendorf, Switzerland), and its chemical formula is represented in Figure 1.

The biopolymer chosen was polycaprolactone (PCL, Mw = 80000 g/mol) and was purchased from Sigma-Aldrich. Its chemical formula is also illustrated in Figure 1.

Regarding the solvents used, 1,1,1,3,3,3-hexafluoro-2-propanol (HFP), dichloromethane (DCM), *N,N*-dimethylformamide (DMF), *N,N*-dimethylacetamide (DMAc) and methanol (MeOH), they were purchased from Merck/Sigma-Aldrich (Darmstadt, Germany). All chemicals were used as received.

2.2. Dipeptide Self-assembled Nanostructures in Solution

To visualize the nanostructures to which the dipeptide self-assembles, a solution was prepared by dissolving 0.80 mg of Cyclo(L-Trp-L-Tyr) in a mixture of solvents 4:2:1 DMF/DMAc/H_2O. This solution was filtered with a membrane with 0.45 μm pore diameter and allowed to grow the nanostructures for a month. A drop of this solution was then placed on a silica slide, and the solvents were slowly evaporated at room temperature and sent for SEM analysis.

To study the optical absorption and photoluminescence spectra, the dipeptide was dissolved in HFP at a concentration of 100 mg/mL. Afterwards, it was diluted in MeOH to the final concentrations depending on the characterization and left at room temperature for 24 h.

2.3. Electrospinning of Nanofibers

For electrospinning, a 10% polymer solution of PCL (w/v) was completely dissolved in DCM at 300 rpm and 35 C. A mixture of solvents DMF/DMAc was used to dissolve Cyclo(L-Trp-L-Tyr) in a 1:5 w/w. This was incorporated into the polymer solution, resulting in a 4:1:1 volume ratio of solvents. At room temperature and for several hours, the obtained solution was stirred at 300 rpm.

The vertical electrospinning used, under ambient conditions, has a high voltage power supply with an electrical potential difference of 18 kV, from Spellmann CZE2000, Bochum, Germany. The tip-of-needle collector distance (TCD) was 11 cm, and a high purity

Preprints (www.preprints.org) | NOT PEER-REVIEWED | Posted: 21 June 2023 doi:10.20944/preprints202306.1571.v1

aluminum foil was placed on the collector to facilitate fiber manipulation and act as an electrode.

Other electrospinning parameters to ensure a stable process and the production of bead-free nanofibers were the flow rate of 0.18 mL/h and a needle with an outer diameter of 0.813 mm (inner diameter 0.508 mm). The syringe was loaded with the polymeric and dipeptide solution and the high voltage power of 18 kV was applied to the tip-of-needle, as seen in Figure 1.

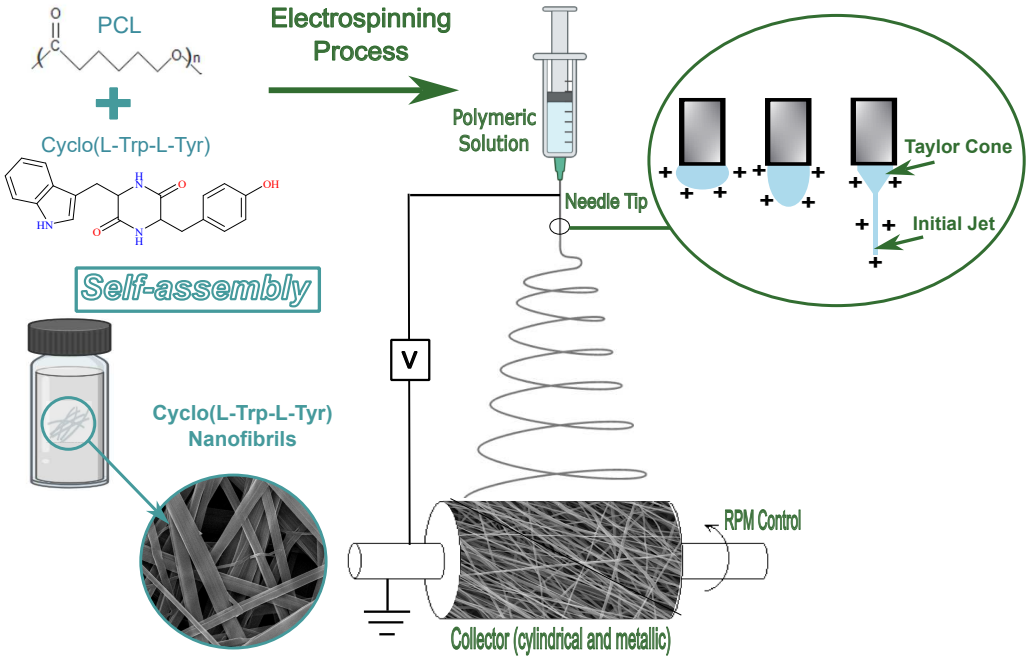

Figure 1. Schematic representation of the electrospinning process and the materials used, both in the production of the Cyclo(L-Trp-L-Tyr)@PCL nanofibers and the self-assembly in solution of the dipeptide.

2.4. Scanning Electron Microscopy (SEM)

To study the morphology of Cyclo(L-Trp-L-Tyr) structures, scanning electron microscopy was performed using a Nova Nano SEM 200 microscope, operated at an accelerating voltage of 10 kV. Slides with Cyclo(L-Trp-L-Tyr) structures in solution and the fiber mat were covered with a 10 nm thick Au-Pd film (80-20 weight%) using a high resolution sputter coater, 208HR Cressington Company, coupled to a high resolution thickness controller, MTM-20 Cressigton. The resulting images were analyzed using ImageJ 1.53k image analysis software (NIH, https://imagej.nih.gov/ij/, February 2023). The distribution and average diameters were calculated by measuring 145 nanofibrils and 88 fibers from the SEM images, and the results were fitted to a log-normal function.

2.5. Confocal Laser Scanning Microscopy

The Olympus^{TM} FluoView FV1000 confocal scanning laser microscope (Olympus, Tokyo, Japan) was used to observe the fluorescence of the nanofibers with a 40x objective, an excitation wavelength of 405 nm and detection filters BA 430 – 470. Confocal images were acquired with 800 $\times$ 800 pixel resolution and a 1 cm^2 fiber mat with 120 μm thickness on a glass slide. The sample was scanned at room temperature.

2.6. Optical Absorption, Photoluminescence and Diffuse Reflectance Spectroscopy (DRS)

Optical absorption (OA) measurements were performed on Cyclo(L-Trp-L-Tyr) solutions and fiber mat using a Shimadzu UV-3600 Plus UV–Vis-NIR spectrophotometer (Shimadzu Corporation, Kyoto, Japan). At room temperature and in the wavelength range

Preprints (www.preprints.org) | NOT PEER-REVIEWED | Posted: 21 June 2023 doi:10.20944/preprints202306.1571.v1

of 200 to 600 nm. The solutions were prepared in methanol and measured in a quartz cuvette with a path length of 1 cm.

From UV-vis absorption spectroscopy, it is possible to determine the optical bandgap energy (E_g) of the nanoparticles, using the Tauc plot given by $(\alpha h\nu)^n = k(h\nu - E_g)$ [23]. Parameters are α, the absorption coefficient; $h\nu$ is the incident photon energy; n, the type of electronic transition and, for this work, $n = 1/2$ as this is an indirect bandgap material; k a constant of proportionality independent of the energy and $k = 1$ (amorphous materials).

The equipment used for the photoluminescence spectra was a Fluorolog 3 spectrofluorimeter (HORIBA Jobin Yvon IBH Ltd., Glasgow, UK), using an excitation wavelength of 280 nm and in the wavelength range of 290 to 600 nm, with input and output slits fixed to provide a spectral resolution of 2 nm. Photoluminescence excitation (PLE) spectra were recorded in the wavelength range of 220 to 300 nm.

For the measurement of the diffuse reflectance spectrum (DRS) of the nanofiber mat, a UV-2501PC spectrophotometer (Shimadzu Corporation, Kyoto, Japan) equipped with an integration sphere, Shimadzu ISR-205 240A was used and barium sulfate was taken as a reference. In the measurement, a wavelength rate of 200 to 800 nm was used with a step size of 1 nm.

To determine the bandgap energy (E_g) of the material, we applied the Kulbelka-Munk function, F(R), to the experimental data. The Kubelka-Munk function is given by $F(R) = (1 - R)^2/2R$, R is the total reflectance coefficient of the material. As such, the bandgap is calculated using the equation $[h\nu F(R)]^{1/2} = \alpha(h\nu - E_g)$ [24].

2.7. Mechanical and Hydrophobic Tests

Mechanical tests were performed on a Zwick/Roell Z005 (ZwickRoell, Germany) universal testing machine (ASTM D882-02). The specimens were cut from electrospun PCL fiber mats (40 x 10 mm) and tested at 25 mm/min, with a gauge length of 26 mm. The mechanical indexes are the average values of at least 7 specimens.

The hydrophilicity of the electrospun PCL fiber mat was measured using a goniometer (Contact Angle System OCA 20 Dataphysics, Germany). Deionized water $(3\,\mu L)$ was automatically dropped onto the flat fibers with a precision syringe, following the sessile drop method. At least 20 measurements were made and the mean value was taken.

2.8. Second Harmonic Generation (SHG)

Second harmonic measurements on the fiber mats were performed using a mode-locked Ti: Sapphire laser (Coherent Mira) as an excitation source. The incident fundamental light was focused onto the fiber mats using a Nikon CFI Plan Fluor x10 objective, see Figure 2. Due to the opacity of the fiber mats, the second harmonic light was detected in reflection (epi-illumination). Although the bandwidth of the fundamental light is sufficient to produce 85 fs pulses (full-width half-maximum), we estimate that dispersion in the optical elements stretches the pulses to approximately 120 fs duration when incident on the samples. For the fibers, incident pulse energies ranged from 65 to 130 pJ. A 1mm thick BBO crystal cut for phase matching at 800 nm was used to calibrate the detection system. For the BBO crystal, the incident pulse energies were 5 to 7 pJ. The second harmonic light was separated from the incident fundamental light by a short-pass dichroic mirror, then it passes through a narrow band-pass filter (Semrock FF01-405/150-25) before being focused onto a fiber bundle coupled to an Andor imaging spectrometer (Shamrock 300i) equipped with a CCD array (Newton) cooled to -50 °C. The signal was integrated for 1 second in the case of the fibers and 4 ms in the case of BBO. The second harmonic spectra were fit to a Gaussian profile as detailed in the supplementary information of [25]. The area under the Gaussian fit was taken as a proxy for the total number of second harmonic signal counts.

Preprints (www.preprints.org) | NOT PEER-REVIEWED | Posted: 21 June 2023 doi:10.20944/preprints202306.1571.v1

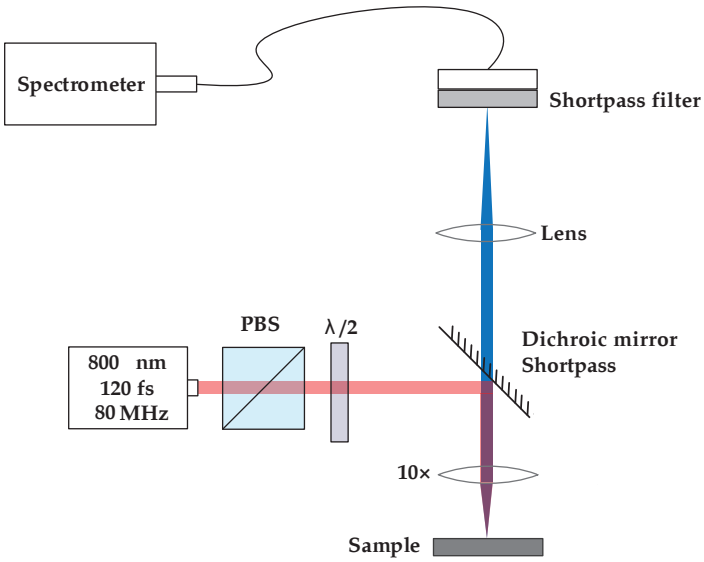

Figure 2. Second harmonic microscope layout. PBS - Polarized beam splitter; $\lambda/2$ - half-waveplate. The transmission of the PBS is aligned vertically.

2.9. Piezoelectric Measurements

The piezoelectric output voltage was measured through a load resistance of 100 MΩ and collected in a digital storage oscilloscope (Agilent Technologies DS0-X-3012A3012A, Waldbronn, Germany) after going through a low-pass filter and a low noise preamplifier (Research systems SR560, Stanford Research Systems, Stanford, CA, USA). The nanofiber sample had a 30 × 40 mm^2 area and a thickness of 120 μm and is placed in thin plates of high purity copper (top: 23 × 30 mm^2 and bottom: 30 × 33 mm^2). Periodic mechanical forces were applied to the fiber array by a vibration generator (Frederiksen SF2185) with a frequency of 3 Hz determined by a signal generator (Hewlett Packard 33120A). Before measuring, it was necessary to calibrate the applied forces with a FSR402 force sensing resistor (Interlink Electronics Sensor Technology, Graefelfing, Germany). The forces applied were uniform and perpendicular to the surface area of the sample.

3. Results and Discussion

3.1. Morphological Characterization

The dipeptide Cyclo(L-Trp-L-Tyr) in a solution of DMF/DMAc/H_2O self-assembles into nanofibrils, as may be seen in the SEM images in Figures 3 **(a)** and **(b)**. These nanofibrils have an average diameter of 218 ± 70 nm as shown in Figure 3 **(c)**. The histogram was constructed from a total of 145 measurements, with the minimum diameter of 87 nm and the maximum 487 nm.

Figures 3 **(d)** and **(e)** are SEM images of the dipeptide embedded into nanofibers, Cyclo(L-Trp-L-Tyr)@PCL, fabricated by the electrospinning technique. These fibers have an average diameter of 417 ± 112 nm and a quite wide diameter distribution from a minimum diameter of 208 nm to a maximum of 696 nm, Figure 3 **(f)**. In Figure 3 **(e)**, it is possible to see nanotubes formed outside the fiber, with an average diameter of 58 ± 13 nm, indicating that in the polymer matrix the dipeptide self-assembles in the form of nanotubes.

In hydrogel form, You Y. and co-authors successfully produced Cyclo(L-Trp-L-Tyr) dipeptide fibrils measuring 100 ± 50 nm in width. Furthermore, they observed interconnected fibrous networks in 3D, formed by these fibrils [26].

In our previous work [16], we verified that the dipeptide Cyclo(L-Trp-L-Trp) self-assembles into nanospheres of an average diameter of 245 nm.

In the present study, we utilized the dipeptide Cyclo(L-Trp-L-Tyr), where the OH group of tyrosine enables the formation of additional hydrogen bonds with both the tryptophan units and among the tyrosine residues. These hydrogen bonds, facilitated by

Preprints (www.preprints.org) | NOT PEER-REVIEWED | Posted: 21 June 2023 doi:10.20944/preprints202306.1571.v1

the OH group of tyrosine, are considered stronger than those formed by the NH group present in tryptophan. This is due to the higher electronegativity of oxygen, found in the OH group, compared to nitrogen in the NH group, resulting in greater attraction of shared electrons in the hydrogen bond [26,27]. Furthermore, the linear geometry adopted by the OH group contributes to a stronger interaction. These combined factors enhance the strength of the hydrogen bonds and promote the formation of a more extensive and organized network, facilitating the formation of nanotubes.

In terms of the electrospun nanofibers, they showed no bead formation, and electrospinning proved to be a stable and appropriate technique for the production of these nanomaterials.

In the article [16], we obtained an average diameter of 600 nm for PCL nanofibers functionalized with Cyclo(L-Trp-L-Trp), and in [28], the electrospun fibers of Boc-Phe-Phe (Boc-L-phenylalanine-L-phenylalanine-OH) formed from PCL resulted in diameters in a range of 590-700 nm. Similar to the ones from the present study.

An additional structural characterization was performed by Fourier transform infrared spectroscopy (FTIR), see Figure S1. The spectra show changes in peak intensity and shape, indicating the successful incorporation of the CDP inside the fibers.

3.2. Optical Absorption, Photoluminescence and Diffuse Reflectance Spectroscopy of Dipeptide Self-assemblies

The UV-vis absorption spectrum of a 0.43 mM Cyclo(L-Trp-L-Tyr) in methanol is depicted in Figure 4 **(a)**, showing an absorption band from 250 to 300 nm with three smaller spikes at 273, 280 and 289 nm. These represent the formation of structures called quantum dots, QDs. As reported in the literature, for the case of Cyclo-FW (cyclo-phenylalanine-tryptophan) and Cyclo-WW (cyclo-tryptophan-tryptophan), the monomers of CDPs form dimeric QDs that act as the foundation for more complex supramolecular structures [8].

The bandgap energy of $E_g = 4.11 \pm 0.01$ eV, was obtained for Cyclo(L-Trp-L-Tyr), from the absorption spectrum, through the Tauc plot; see the inset in Figure 4 **(a)**. The obtained value agrees with those reported from density functional theory (DFT) for Cyclo-FW and Cyclo-WW, which have bandgap energies of 3.63 eV and 3.56 eV, respectively [8].

In Figure 4 **(b)**, it is possible to verify the match between the absorption spectrum and the photoluminescence excitation (PLE) spectrum of the dipeptide in solution, for excitation at a maximum wavelength of 280 nm.

The photoluminescence (PL) emission spectrum of the 0.001 mM dipeptide solution in MeOH, for excitation at 280 nm, is represented in Figure 4 **(b)** with maximum emission peak at 311 nm. The PL spectrum of Cyclo(L-Trp-L-Tyr)@PCL nanofibers is represented in blue, also in Figure 4 **(b)**, with a maximum at 330 nm and another, less intense emission peak at 440 nm, in the blue region of the optical spectra, that might indicate the presence of larger dipeptide nanostructures. The shift observed in the PL spectrum, from 311 nm for a dipeptide solution to 330 nm when the dipeptide is embedded into the nanofiber is representative of an increase in the size of the nanostructures incorporated into the nanofibers.

As a further study of the nanofibers, the diffuse reflectance spectrum (DRS) was measured for Cyclo(L-Trp-L-Tyr)@PCL and compared with the fiber mat without embedded dipeptide, in Figure 4 **(c)**. The spectrum shows two peaks of minimum reflectance at 283 and 330 nm. The bandgap energies obtained for the dipeptide nanostructures both in solution and embedded into the electrospun fibers are approximately 4.0 eV, which are expected values for organic wide-bandgap semiconductors [29].

The bandgap energy values obtained in this study for Cyclo(L-Trp-L-Tyr) are also similar to those reported in a previous work with Cyclo(L-Trp-L-Trp) in solution and in fibers [16].

Preprints (www.preprints.org) | NOT PEER-REVIEWED | Posted: 21 June 2023 doi:10.20944/preprints202306.1571.v1

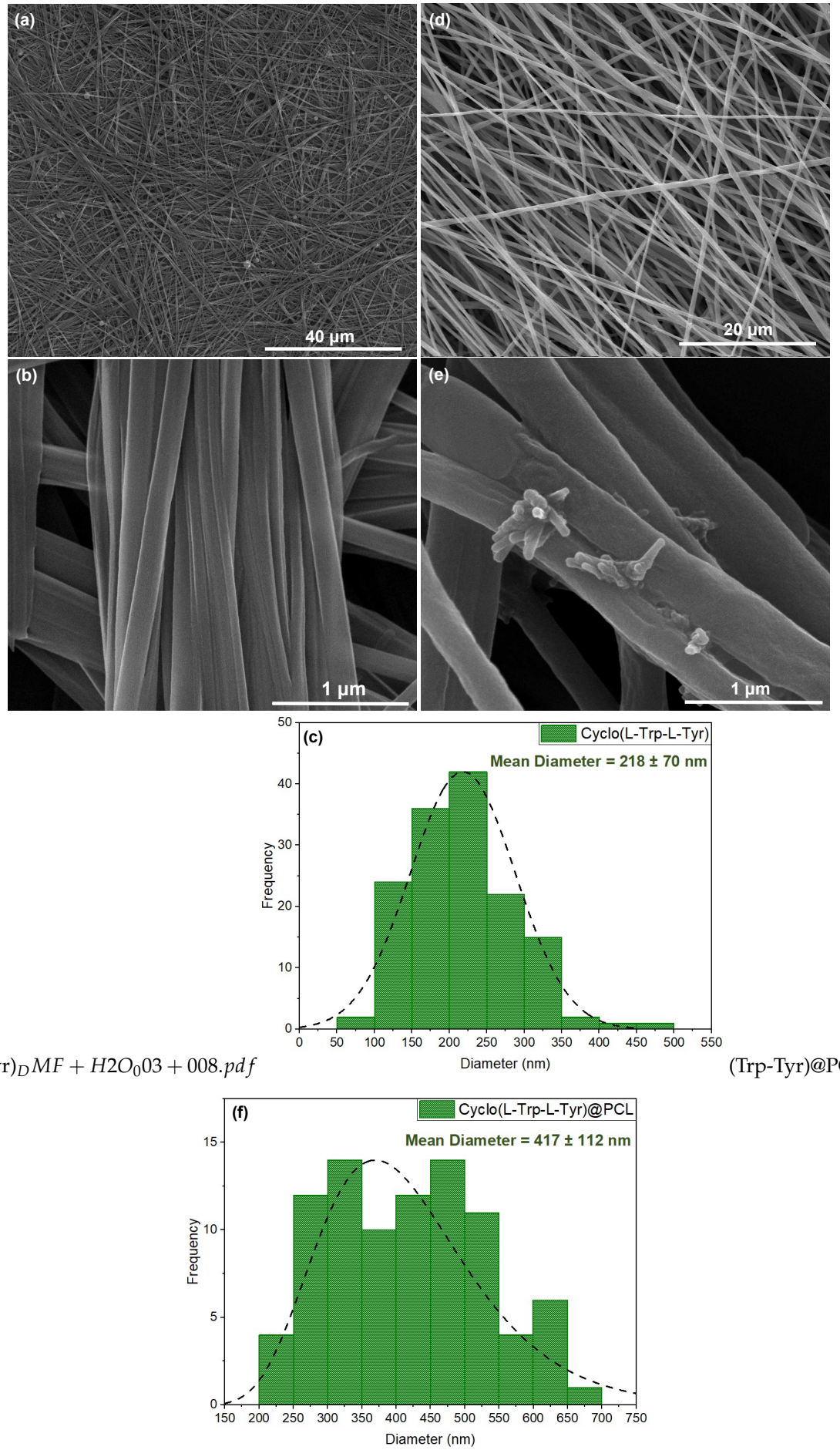

$(\text{Trp-Tyr})_D MF + H2O_0 03 + 008.pdf$

(Trp-Tyr)@PCL.pdf

Figure 3. SEM images of Cyclo(L-Trp-L-Tyr): (**a**) and (**b**) as self-assembled nanofibrils in a solution of DMF/DMAc/H_2O at a magnification of 2,500x and 50,000x, respectively; (**d**) and (**e**) as nanofibers produced by electrospinning with Cyclo(L-Trp-L-Tyr) embedded into the biopolymer PCL at a magnification of 5,000x and 100,000x. The respective diameter histograms of the nanofibrils (**c**) and

Preprints (www.preprints.org) | NOT PEER-REVIEWED | Posted: 21 June 2023 doi:10.20944/preprints202306.1571.v1

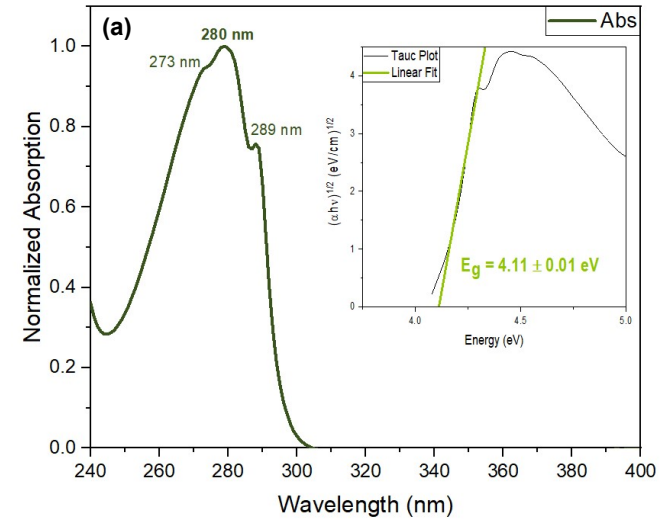

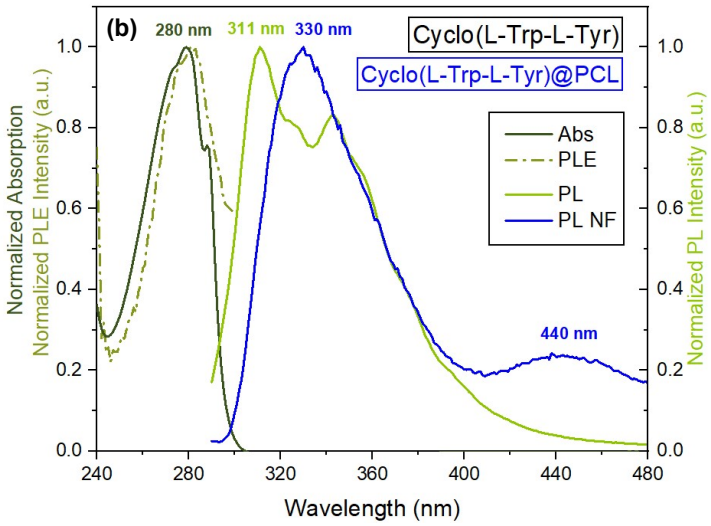

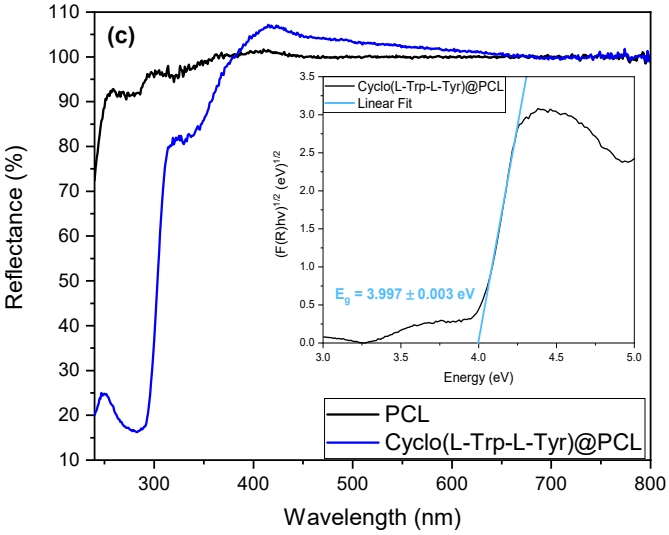

40x a3 3x digital zoom.pdf

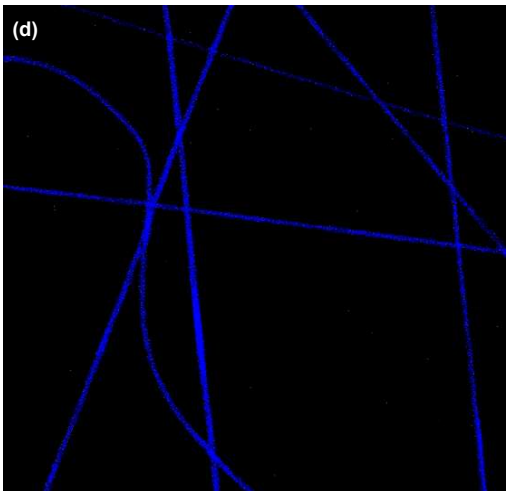

Figure 4. (**a**) Normalized UV-vis absorption spectrum with the bandgap energy obtained from the calculation of the Tauc plot (inset). (**b**) Normalized UV-vis absorption, photoluminescence excitation (PLE), photoluminescence (PL) of Cyclo(L-Trp-L-Tyr) in MeOH and PL spectra of Cyclo(L-Trp-L-Tyr)@PCL nanofibers. (**c**) DRS of Cyclo(L-Trp-L-Tyr)@PCL, inset represents the bandgap obtained from the Kubelka-Munk function. (**d**) Confocal microscopy image of the Cyclo(L-Trp-L-Tyr)@PCL nanofiber mat, under a laser excitation of 405 nm.

Preprints (www.preprints.org) | NOT PEER-REVIEWED | Posted: 21 June 2023 doi:10.20944/preprints202306.1571.v1

3.3. Mechanical and Hydrophobic Properties of Electrospun Fibers

In Figure 5, the mechanical properties of PCL fibers are presented, with stress-strain curves indicating that the incorporation of CDPs increases stiffness. On average, the elastic modulus (Young's modulus) increased by 445% (from 6.9 to 37.6 MPa) and the tensile strength by 72% (from 1.5 to 2.6 MPa), while the elongation at break was reduced by 35% (from 121 to 79%). Additionally, in previous studies, a notable improvement in the mechanical characteristics of the polymers was observed with the integration of organic crystals, specifically involving polyvinyl chloride (PVC) and PLLA [16,30,31].

The cyclo-dipeptides effectively transfer applied forces between the polymer and nanotubes, reinforcing the polymeric matrix. This behavior is similar to that observed for electrospun polymer fibers embedded with nanospheres of the Cyclo(L-Trp-L-Trp) dipeptide [16] where the fiber mechanical properties were improved. These results, an increase of the elastic modulus and an elongation at break, are beneficial to the piezoelectric response of the material, enabling the fiber mat to withstand greater forces and deformations. The Young's modulus was found to depend significantly on the angle between the stretch direction and the fiber direction [32], in our case the functional electrospun fibers were stretched along the longitudinal axis of the fiber. Our previous work also demonstrates that the incorporation of lead-free organic ferroelectric perovskite N-methyl-N'-diazabicyclo [2.2.2]octonium)-ammonium triiodide (MDABCO-NH_4I_3) nanocrystals in polyvinyl chloride microfibers [31] resulted in an improvement in Young's modulus compared to polymer electrospun fibers with no embedded material.

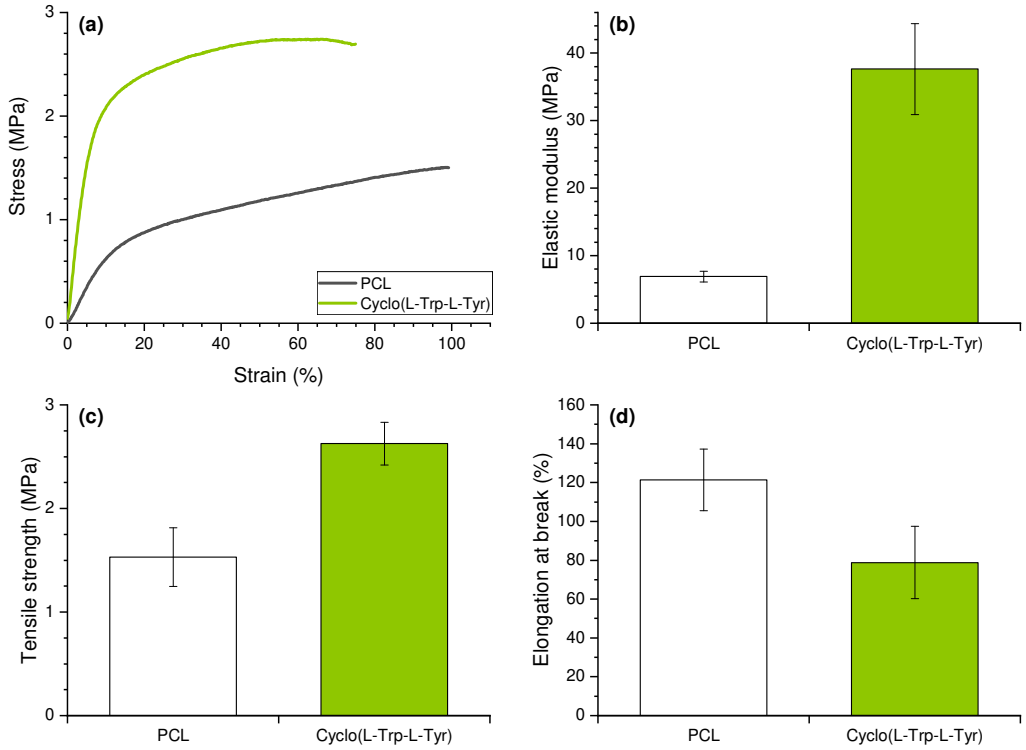

Figure 5. (a) Representative tensile curves, **(b)** Elastic modulus (Young's modulus), **(c)** Tensile strength and **(d)** Elongation at break of the electrospun nanofibers of PCL (grey) and Cyclo(L-Trp-L-Tyr)@PCL (green).

The hydrophilic/hydrophobic characteristics of biodegradable polymers can be determined by their absorption of water, which in turn affects their susceptibility to degradation by hydrolytic processes. It is known that PCL is a hydrophobic polymer [33,34].

Figure 6 shows the contact angles of PCL fibers and Cyclo(L-Trp-L-Tyr)@PCL fibers, and it is possible to notice a significant reduction in the hydrophobicity of PCL fibers after the incorporation of Cyclo(L-Trp-L-Tyr) nanotubes. This reduction is due to the presence

Preprints (www.preprints.org) | NOT PEER-REVIEWED | Posted: 21 June 2023 doi:10.20944/preprints202306.1571.v1

of a large number of hydroxyl groups (-OH) and a wide network of hydrogen bonds established in the peptide nanostructures that strongly bind to water molecules. When water molecules are adsorbed by the peptide nanostructures of Cyclo(L-Trp-L-Tyr), they can form highly mobile hydrogen ions that facilitate the transfer of electrical charge through the material. This mobility of hydrogen ions might increase in electrical conductivity of the material in response to higher levels of humidity.

Furthermore, the thermal behavior of Cyclo(L-Trp-L-Tyr) dipeptide, Cyclo(L-Trp-L-Tyr)@PCL and PCL nanofibers was tested by thermogravimetric analysis (see Figure S2) and differential scanning calorimetry (Figure S3). The findings presented herein suggest that the introduction of the dipeptide had an insignificant effect on the thermal properties of the biopolymer. Notably, the thermal stability of the polymer matrix enables it to withstand temperatures up to 405 ^{o}C without undergoing degradation. This remarkable attribute makes it highly suitable for the envisaged technological applications.

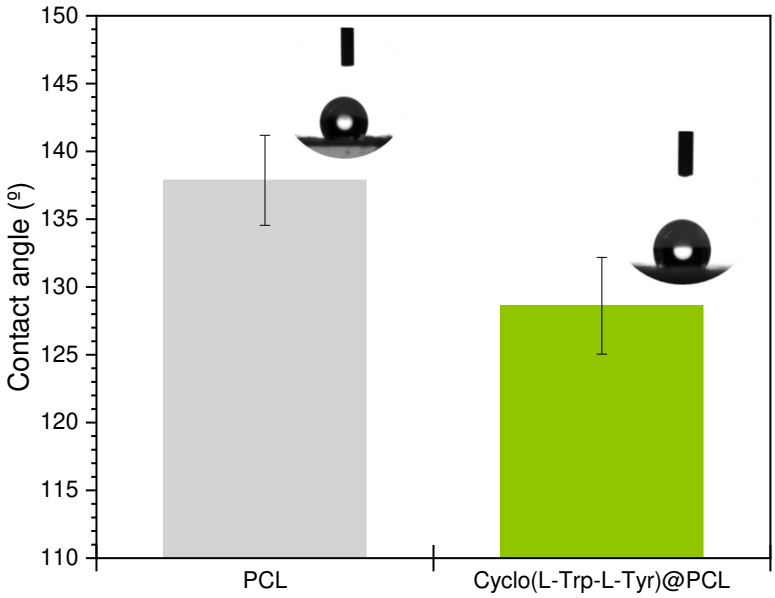

Figure 6. Contact angle of PCL (grey) and Cyclo(L-Trp-L-Tyr)@PCL (green) nanofibers.

3.4. Second Harmonic Generation of Nanofibers

To estimate the effective second-order nonlinear susceptibility, d_{eff}, of the Cyclo(L-Trp-L-Tyr) nanocrystals embedded in the PCL fibers, the second harmonic light measured in reflection from the fibers was compared to that generated by a 1 mm thick orientated beta barium borate (BBO) crystal.

For the calibration signal, a 10x microscope objective (CFI Plan Fluor from Nikon) was used to focus the 4 mm diameter incident fundamental beam within the BBO crystal. Given the effective focal length of 20 mm, we estimate the beam waist at focus is approximately 2.5 μm leading to a Rayleigh length (in air) of $z_R = 25$ μm. Under conditions of strong spatial walk-off due to birefringence, the heuristic model of Wang and Wiener [35] predicts that the second harmonic generation efficiency for an ultrafast pulse will obey the following equation:

$$\eta_{2\omega}^{BBO} \equiv \frac{U_{2\omega}^{BBO}}{U_{\omega}^{BBO}} = \frac{\left[2\omega d_{eff}^{BBO}\right]^2}{n_{\omega} n_{2\omega} \lambda_0 c^3 \varepsilon_0} \pi \sqrt{\frac{\ln 2}{2}} l_S^{BBO} \frac{U_{\omega}^{BBO}}{t_p}$$

Here $U_{2\omega}$ and U_{ω} are, respectively, the energies of the generated second harmonic and incident fundamental pulses, t_p is the full-width half-maximum incident pulse duration (which we estimate to be approximately 120 fs). At the phase matching angle, the refractive

Preprints (www.preprints.org) | NOT PEER-REVIEWED | Posted: 21 June 2023 doi:10.20944/preprints202306.1571.v1

indices of the fundamental and second harmonic light are $n_\omega = n_{2\omega} = 1.66$, while for incident fundamental light at 800 nm $d_{eff}^{BBO} = 2.0$ pm/V [36]. The parameter l_S^{BBO} is an effective crystal thickness given by the ratio of the focused beam waist to the walk-off angle of the second harmonic light $\rho = 69$ mrad that propagates as an extraordinary wave. We estimate that $l_S^{BBO} \simeq 36$ μm.

On the other hand, since the Cyclo(L-Trp-L-Tyr)@PCL fibers have a thickness of the order of the fundamental wavelength, one can invoke the standard plane-wave result for second harmonic generation leading to an efficiency given by

$$\eta_{2\omega}^{Cyclo(L-Trp-L-Tyr)@PCL} \equiv \frac{\left[2\omega\, d_{eff}^{Cyclo(L-Trp-L-Tyr)@PCL}\right]^2}{n_\omega n_{2\omega} \lambda_0 c^3 \varepsilon_0} \sqrt{\frac{\ln 2}{2\pi}} \frac{U_\omega^{Cyclo(L-Trp-L-Tyr)@PCL} s^2_{Cyclo(L-Trp-L-Tyr)@PCL}}{z_R\, t_p}$$

Here $s_{Cyclo(L-Trp-L-Tyr)@PCL}$ is the thickness of the illuminated Cyclo(L-Trp-L-Tyr) crystal embedded in the PCL fibers. Taking the ratio between these two efficiencies, we can solve the effective nonlinear susceptibility of the Cyclo(L-Trp-L-Tyr) nanocrystals,

$$d_{eff}^{Cyclo(L-Trp-L-Tyr)@PCL} \simeq d_{eff}^{BBO} \left(\frac{U_\omega^{BBO}}{U_\omega^{Cyclo(L-Trp-L-Tyr)@PCL}} \right) \sqrt{\frac{U_{2\omega}^{Cyclo(L-Trp-L-Tyr)@PCL}}{U_{2\omega}^{BBO}}}\, \pi^{3/4} \frac{\sqrt{z_R\, l_{SWO}^{BBO}}}{s_{Cyclo(L-Trp-L-Tyr)@PCL}}$$

We have simplified the above by neglecting small differences between the refractive indices of the BBO and the Cyclo(L-Trp-L-Tyr) nanocrystals. Finally, due to the opaqueness of the fiber mats, we measured the second harmonic generation from the fiber mats in reflection. Since the above expression is for transmission, it was also necessary to calibrate the relative efficiency between the transmission and reflection geometries. Using the BBO crystal we found that the second harmonic signal measured in transmission was approximately 47x larger than that in reflection.

Rather than measuring directing the second harmonic signal energies, we used the amplitude of a Gaussian fit to the acquired second harmonic spectra as a proxy. An example of a fit to the second harmonic light generated by the fiber mat is shown below in Figure 7, where the small and random nature of the residuals is evident.

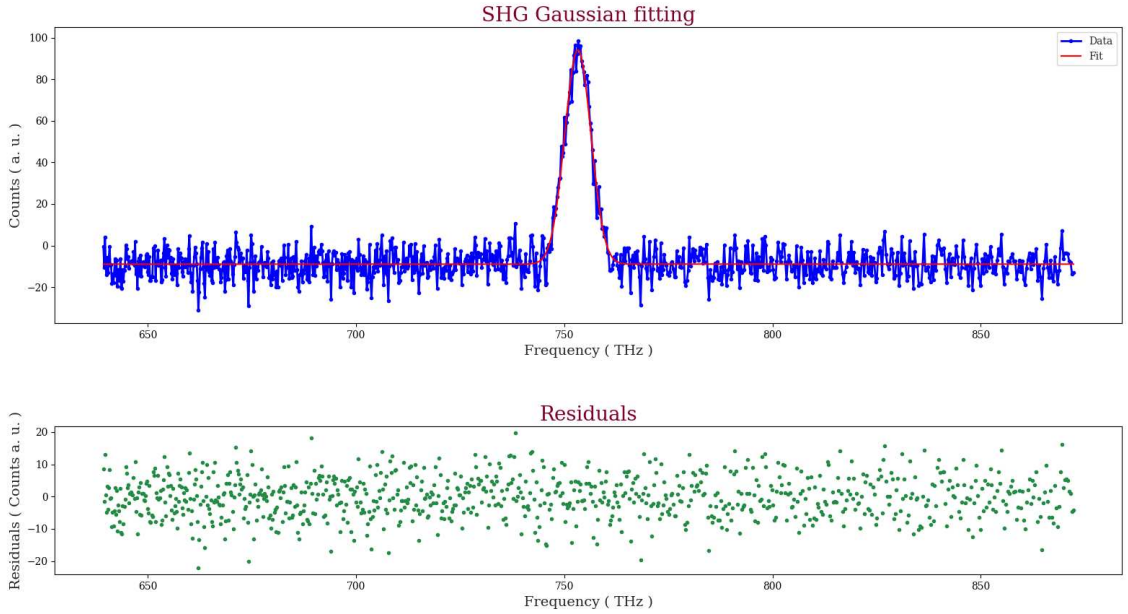

Figure 7. Gaussian fit for the SHG signal from the Cyclo(L-Trp-L-Tyr)@PCL fiber mat.

Preprints (www.preprints.org) | NOT PEER-REVIEWED | Posted: 21 June 2023 doi:10.20944/preprints202306.1571.v1

The measurements carried out on BBO in transmission were taken with an average incident energy of 5.3 pJ per pulse with a pulse repetition rate of 76 MHz. The second harmonic spectra were integrated over 4ms and the Gaussian fits to the spectra gave an average count rate at the spectral peak of 8.3×10^6 counts/s. For the Cyclo(L-Trp-L-Tyr)@PCL fiber mat, a higher incident energy of 129 pJ. The second harmonic spectra were integrated over 1 second and the count rate at the spectral peak was measured to be approximately 102 counts/s. We note however that a single fiber has an average diameter of 417 nm, much smaller than the incident fundamental beam waist of 2.5 mm. We found that significant second harmonic generation from the fiber mats was observed only at select positions, which leads us to hypothesize that only a few fibers contain Cyclo(L-Trp-L-Tyr) nanocrystals with the correct orientation to generate significant second harmonic light. Assuming that the second harmonic signal from the fiber mats is dominated by a single fiber illuminated in the beam waist, the effective incident energy should be reduced by the ratio of the fiber cross-section to the transverse profile, weighted by the Gaussian spatial profile of the incident beam which we estimate to be roughly 0.13. Putting all the measurements together we estimate that the effective second-order nonlinear susceptibility of the Cyclo(L-Trp-L-Tyr) nanocrystals is

$$d_{eff}^{Cyclo(L-Trp-L-Tyr)@PCL} \simeq 0.36 \pm 0.13 \ pm/V$$

In this estimate, the uncertainty arises solely from the estimated standard deviation of the fiber diameters (112 nm).

This result is approximately three times greater compared to the effective second-order nonlinear susceptibility value of the dipeptide glycyl-L-alanine hydroiodide monohydrate (Gly-L-Ala.HI.H_2O) crystals [25].

3.5. Piezoelectric Response of Cyclo(L-Trp-L-Tyr) Nanofibers

Due to its chirality, crystalline Cyclo(L-Trp-L-Tyr) is piezoelectric. In the functionalized fibers piezoelectricity arises mainly from the dipeptide, as it is known that the biopolymer PCL is not piezoelectric.

The voltage and current obtained from a Cyclo(L-Trp-L-Tyr)@PCL fiber mat was measured when perpendicular periodic forces were applied to the sample. Due to the transformation of mechanical energy into an electrical response, as shown in Figure 8 **(b)** (see the inset). The application of periodic forces on the fiber mat, causes a reorientation of the molecular dipoles inside the crystalline material accompanied by a charge separation which originates an output voltage across the active material and finally an electric current is generated through the external circuit.

Figure 8 shows that electrospun PCL nanofibers when funcionalized with Cyclo(L-Trp-L-Tyr) behave as a piezoelectric nanogenerator (PENG).

The maximum value of the measured output voltage was 10.5 V and the maximum piezoelectric current was 105 nA, for a maximum applied force of 4.8 N, see Figure 8 **(a)**. Figure 8 **(b)** shows the linear proportionality between the piezoelectric current and the applied periodical forces.

To determine the piezoelectric coefficient, the following steps were followed: the piezoelectric charge (Q) is calculated from the piezoelectric current I, $Q = \int Idt \ (C)$, considering a response time of 0.001 s. Defining $d_{eff} = Q/F$ (pCN^{-1}), the effective piezoelectric coefficient for the Cyclo(L-Trp-L-Tyr)@PCL nanofibers is 22 pCN^{-1}. In Table 1, this quantity, obtained from the measured electric current, is presented for several dipeptides for comparison. It is also mentioned, in Table 1, that for an electrospun fiber mat fabricated with lead-free organic–inorganic perovskite N-methyl-N'-diazabicyclo [2.2.2]octonium)–ammonium triiodide (MDABCO-NH_4I_3) with PMMA (poly(methyl methacrylate)), $d_{eff} = 64$ pCN^{-1} [31].

In a previous study [16], for the dipeptide Cyclo(L-Trp-L-Trp) incorporated in PCL fibers, the piezoelectric coefficient obtained was 30 pCN^{-1} (Table 1), slightly higher than the value obtained in this work but within the same order of magnitude.

Preprints (www.preprints.org) | NOT PEER-REVIEWED | Posted: 21 June 2023 doi:10.20944/preprints202306.1571.v1

It is interesting to compare the effective piezoelectric coefficient obtained for Cyclo(L-Trp-L-Tyr)@PCL with that of Boc (N-*tert*-butoxycarbonyl) protected linear dipeptide, Boc-L-phenylalanyl-L-tyrosine, embedded in the poly(L-lactic acid) (PLLA) fibers, which is around 7 pCN^{-1} [37], three times smaller. The results presented in Table 1 allow the conclusion that cyclic dipeptides embedded into electrospun fibers display higher piezoelectric properties that the correspondent dipeptides under the form of polycrystalline powder and are also more advantageous that linear dipeptides to be used in energy harvesting devices through the piezoelectric effect.

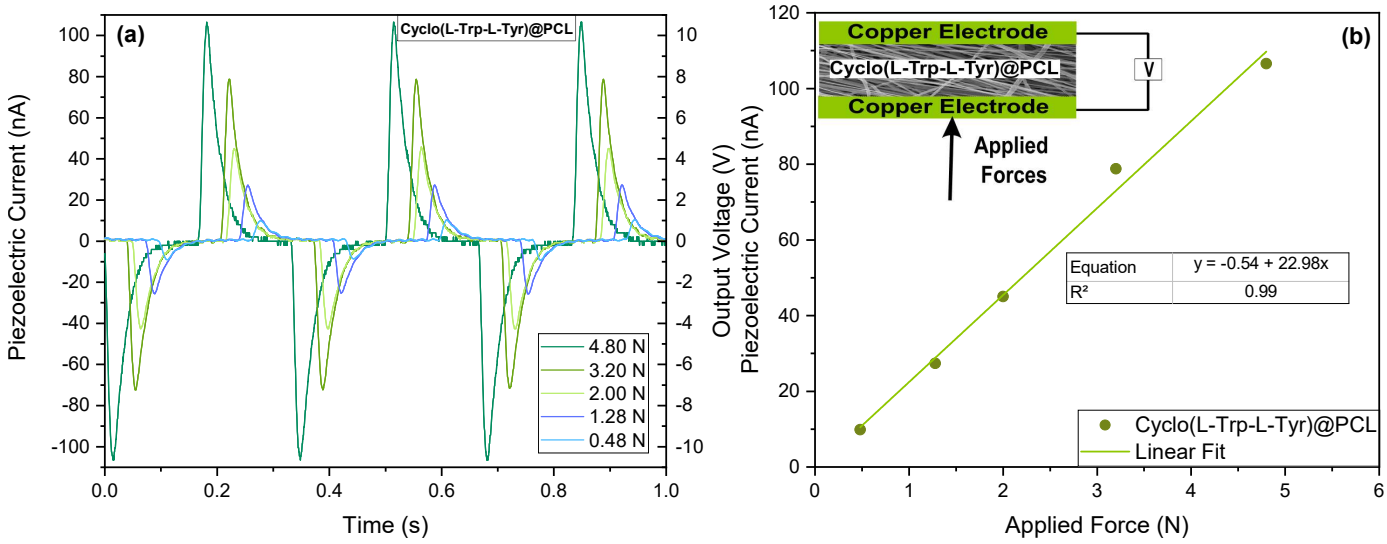

Figure 8. (a) Piezoelectric current and output voltage as functions of time; **(b)** maximum piezoelectric current as a function of the different periodical forces applied to Cyclo(L-Trp-L-Tyr)@PCL nanofibers (inset shows the schematic representation of the PENG).

Preprints (www.preprints.org) | NOT PEER-REVIEWED | Posted: 21 June 2023 doi:10.20944/preprints202306.1571.v1

Table 1. Piezoelectric parameters for application in a nanogenerator based on organic compounds.

Piezoelectric Nanogenerator (PENG)	d_{eff} (pC/N)	V_{out} (V)	Force/Area (N/m^2)	Power Density $(\mu W cm^{-2})$	Ref.
Cyclo(L-Trp-L-Tyr)@PCL (1:5) (fiber mat)	22	10.5	7×10^3	0.16	This work
Cyclo(L-Trp-L-Trp)@PLLA (1:5) (fiber mat)	57	11.5	3×10^3	0.18	[16]
Cyclo(L-Trp-L-Trp)@PCL (1:5) (fiber mat)	30	9.6	5×10^3	0.13	[16]
Cyclo(FW) (crystal powder)	16 [1]	1.4	6×10^5	0.003	[11]
Cyclo(GW) (crystal powder)	5.6 [2]	1.2	7×10^5	0.002	[13]
MDABCO-NH_4I_3@PMMA (1:5) (fiber mat)	64	6.1	11×10^3	0.09	[31]
Boc-PheTyr@PLLA (fiber mat)	7	24	4×10^3	1.0	[37]

[1] Calculated from data available in [11] and assuming a time response of 0.5 s for the nanogenerator; [2] Calculated from data in [13].

4. Conclusions

In this study, we report that the cyclic dipeptide L-Tryptophan-L-Tyrosine self-assembles as nanofibrils when in solution. The incorporation in a biopolymeric matrix, by electrospinning, forms a flexible and mechanically resistant fiber mat, which self-assembled as nanotubes, showing intense blue photoluminescence.

This tryptophan-based aromatic cyclic dipeptide is a wide-bandgap semiconductor, with 4.0 eV of bandgap energy, both in solution and when incorporated into the electrospun nanofibers.

Additionally, the Cyclo(L-Trp-L-Tyr)@PCL fibers demonstrate great potential as optical second harmonic nanogenerators as they present a nonlinear optical effective coefficient of 0.36 pm/V. This value is approximately six times lower than the corresponding coefficient observed in a phase-matched inorganic BBO single crystal.

In order to investigate the feasibility of using this chiral cyclo-dipeptide as a piezoelectric energy harvesting device, periodic forces were applied to the fiber mat, revealing a strong effective piezoelectric coefficient of 22 pCN^{-1}.

The obtained results provide evidence for the considerable potential of the cyclic dipeptide L-Tryptophan-L-Tyrosine, when incorporated into electrospun PCL nanofibers, as optical devices and as nanogenerators for energy harvesting technologies.

Supplementary Materials: The following supporting information can be downloaded at: https://www.mdpi.com/article/10.3390/1010000/s1, Figure S1: FTIR spectra; Figure S2: TGA spectra; Figure S3: DSC spectra. References [38,39] are cited in the supplementary materials.

Author Contributions: Conceptualization, D.S., R.M.F.B. and E.d.M.G.; investigation, D.S., R.M.F.B., A.H., B.A., P.V.R., C.C., A.M. and M.J.L.F.R.; writing—original draft preparation, D.S., R.M.F.B. and E.d.M.G.; writing—review and editing, R.M.F.B., E.d.M.G., B.A. and M.B.; supervision, R.M.F.B., E.d.M.G. and B.A.; project administration, R.M.F.B. and B.A.; funding acquisition, R.M.F.B. and B.A. All authors have read and agreed to the published version of the manuscript.

Funding: This research was funded by Fundação para a Ciência e Tecnologia through FEDER (European Fund for Regional Development)-COMPETE-QREN-EU (ref. UID/FIS/04650/2013 and UID/FIS/04650/2019) and E-Field"Electric-Field Engineered Lattice Distortions (E-FiELD) for optoelectronic devices, ref. PTDC/NAN-MAT/0098/2020.

Institutional Review Board Statement: This study did not involve humans or animals.

Informed Consent Statement: This study did not involve humans or animals.

Data Availability Statement: Not applicable.

Acknowledgments: We acknowledge national funds (OE), through FCT - Fundação para a Ciência e a Tecnologia, I.P., in the scope of the framework contract foreseen in the numbers 4, 5, and 6 of Article 23, of the Decree-Law 57/2016, of August 29, changed by Law 57/2017, of July 19.

Conflicts of Interest: The authors declare no conflict of interest.

Supplementary Information

S1. Attenuated Total Reflectance Fourier Transform Infrared Spectroscopy (FTIR-ATR)

Fourier transformed infrared analysis of electrospun PCL, Cyclo(L-Trp-L-Tyr)@PCL fibers and Cyclo(L-Trp-L-Tyr) powder was recorded on a Jasco 4100 FTIR spectrometer in transmittance mode, in the range of 4000 to 600 cm^{-1}, averaging 32 scans and using a resolution of 8 cm^{-1}. FTIR data were treated with OriginPro 2018 SR1 software (OriginLab Corporation, Northampton, MA, USA).

As depicted in Figure S1, after the integration of the cyclo-dipeptide into the PCL fibers, a reduction in intensity is evident in the FTIR spectra of the dipeptide peaks. This phenomenon can be attributed to the intermolecular interaction occurring between the dipeptide and the polymeric matrix. Nevertheless, no noteworthy disparities in the vibrational frequencies of these peaks were detected, signifying that the structural integrity of the cyclo-dipeptide remains intact subsequent to its self-assembly into nanotubes encapsulated within the PCL nanofibers.

The reduction in intensity of the FTIR peaks can be attributed to the transfer of vibrational energy from the cyclo-dipeptide to the polymeric matrix. This molecular interaction leads to a decrease in the energy absorption of the sample, consequently resulting in diminished intensity of the peaks observed in the FTIR spectra. An additional factor to consider is that electrospun nanofibers consist of a dipeptide:polymer ratio of 1:5, which may contribute to the diminished intensity observed in the peaks.

Certain peaks within the range of 1100 – 3400 cm^{-1} were successfully assigned. The stretching band of the amide group (C = O) in the peptide was observed at 1660 cm^{-1}, corresponding to a β-sheet arrangement of Cyclo(L-Trp-L-Tyr) molecules [27,38]. The stretching band of the N–H bond in Cyclo(L-Trp-L-Tyr) monomers appears as a narrow peak at 3363 cm^{-1} and as a broad and less intense band when self-assembled within PCL fibers (Cyclo(L-Trp-L-Tyr)@PCL), attributed to the N–H/O–H stretching vibrations, between cyclo-dipeptide molecules (L-Trp-L-Tyr). At approximately 1107 cm^{-1}, a peak indicative of the C = C stretching vibration is observable, while another peak can be observed at 1234 cm^{-1} corresponding to the C–N stretching vibration [26,27].

Preprints (www.preprints.org) | NOT PEER-REVIEWED | Posted: 21 June 2023 doi:10.20944/preprints202306.1571.v1

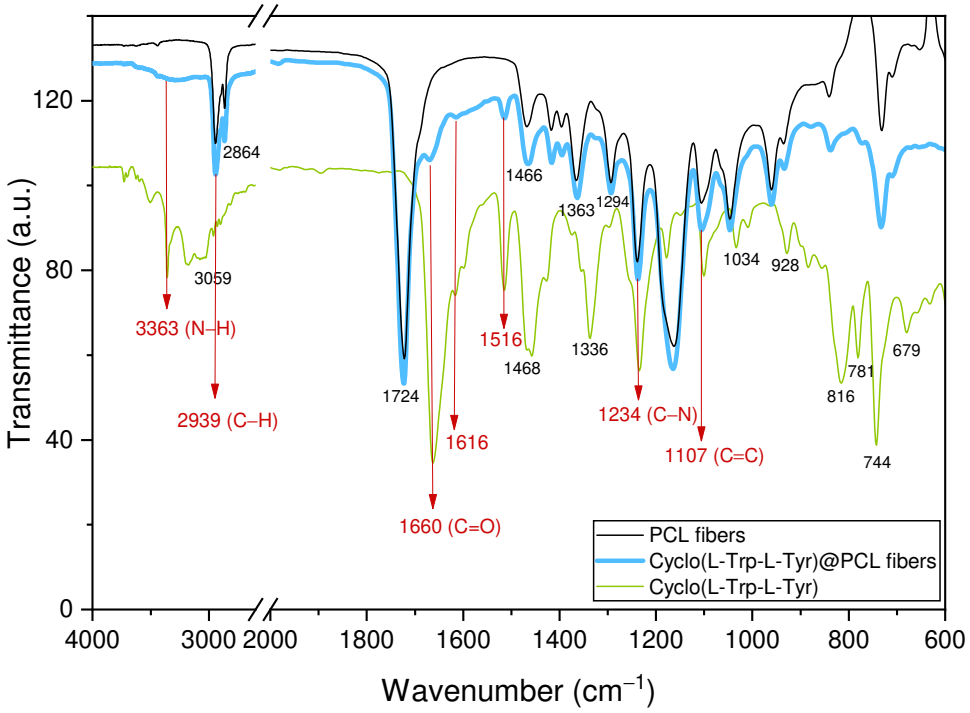

Figure S1. FTIR spectra of the Cyclo(L-Trp-L-Tyr) powder, the polymer (PCL) and Cyclo(L-Trp-L-Tyr)@PCL nanofibers.

S2. Thermogravimetric Analysis (TGA) and Differential Scanning Calorimetry (DSC)

Thermogravimetric analysis (TGA) of the fibers and powder was accomplished using a TGA Q500 (TA Instruments, New Castle, USA) under nitrogen atmosphere at 10 °C/min in a temperature range from 40 to 600 °C. The thermal behavior was analyzed using a DSC Netzsch 200 Maya (Netzsch, Selb, Germany). The tests were carried out under nitrogen atmosphere with a heating rate of 2 °C/min from 25 to 200 °C.

The TGA spectrum of the Cyclo(L-Trp-L-Tyr) dipeptide reveals a small initial mass loss of 3% occurring at 108 °C, corresponding to the loss of residual water. Above 393 °C, a considerable mass loss of approximately 76% is observed, related to the degradation of the dipeptide. The fusion followed by complete degradation of the PCL fibers, resulting in a mass loss of 97%, occurs at 405 °C, as reported previously [13,34,39]. The PCL fibers incorporated with the dipeptide exhibit complete degradation at 397 °C, with a mass loss of 95%, indicating a slight decrease in thermal stability compared to the PCL fibers without the dipeptide, see Figure S2.

Preprints (www.preprints.org) | NOT PEER-REVIEWED | Posted: 21 June 2023 doi:10.20944/preprints202306.1571.v1

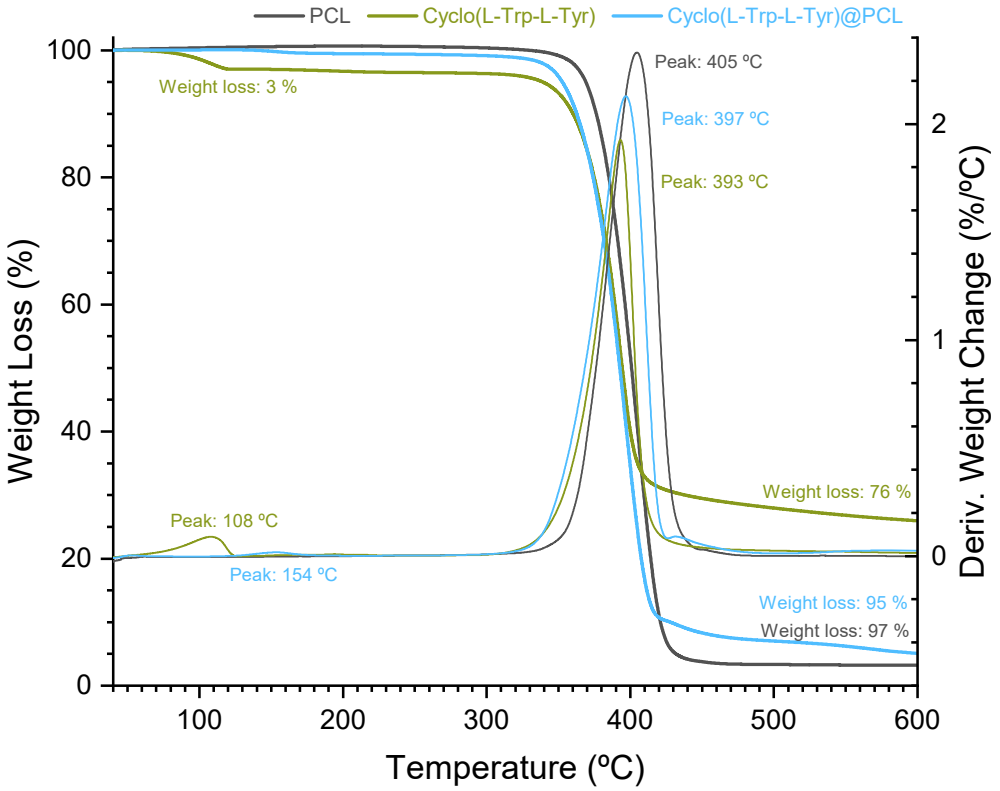

Figure S2. TGA spectra of Cyclo(L-Trp-L-Tyr) dipeptide, Cyclo(L-Trp-L-Tyr)@PCL and PCL fibers.

Figure S3 shows the DSC analysis, it was determined that the incorporation of the dipeptide had no significant effect on the glass transition temperature (T_g) of PCL, which occurs for both at around 60 C, this value is corroborated in literature [39]. The dipeptide remains stable within the measured temperature range and does not exhibit any changes in physical state, such as solid-liquid phase transitions or alterations in molecular or crystalline arrangement.

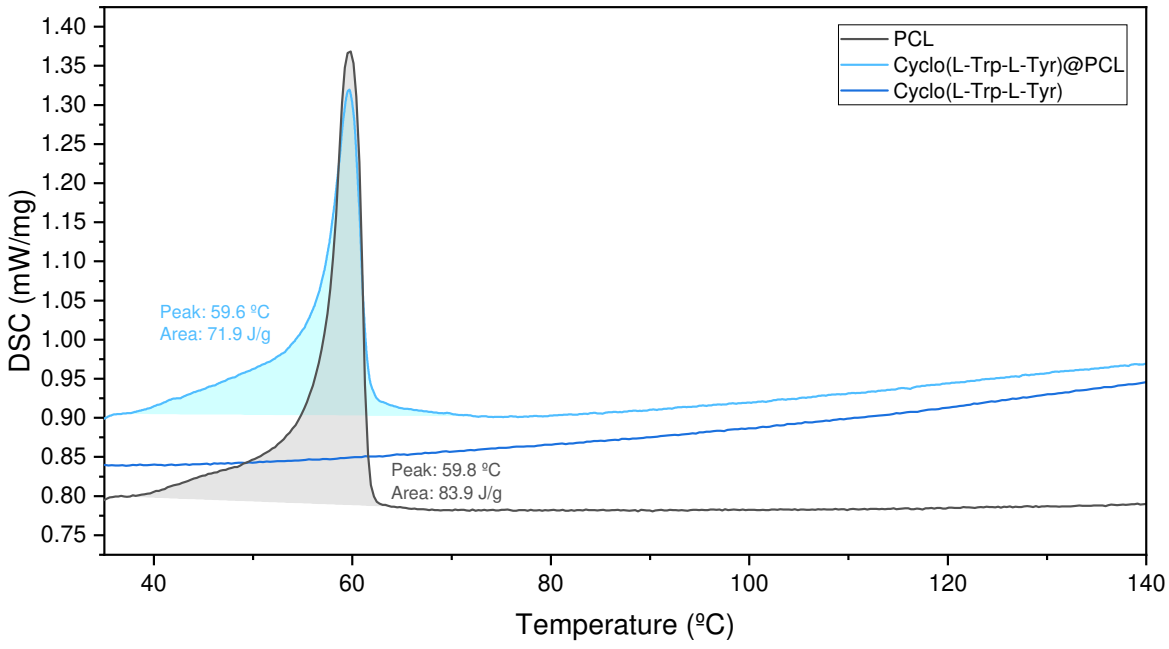

Figure S3. DSC spectra of Cyclo(L-Trp-L-Tyr) dipeptide, Cyclo-(L-Trp-L-Tyr)@PCL and PCL fibers.

References

1. Sim, S.; Wong, N. Nanotechnology and Its Use in Imaging and Drug Delivery (Review). *Biomedical Reports* **2021**, *14*, 42. https://doi.org/10.3892/br.2021.1418.
2. Chen, X.; Xu, S.; Yao, N.; Shi, Y. 1.6 V Nanogenerator for Mechanical Energy Harvesting Using PZT Nanofibers. *Nano Letters* **2010**, *10*, 2133–2137. https://doi.org/10.1021/nl100812k.
3. Taran, M.; Safaei, M.; Karimi, N.; Almasi, A. Benefits and Application of Nanotechnology in Environmental Science: An Overview. *Biointerface Research in Applied Chemistry* **2020**, *11*, 7860–7870. https://doi.org/10.33263/BRIAC111.78607870.
4. Gazit, E. Self-Assembled Peptide Nanostructures: The Design of Molecular Building Blocks and Their Technological Utilization. *Chemical Society Reviews* **2007**, *36*, 1263. https://doi.org/10.1039/b605536m.
5. Manchineella, S.; Govindaraju, T. Molecular Self-Assembly of Cyclic Dipeptide Derivatives and Their Applications. *ChemPlusChem* **2017**, *82*, 88–106. https://doi.org/10.1002/cplu.201600450.
6. Chen, Y.; Tao, K.; Ji, W.; Makam, P.; Rencus-Lazar, S.; Gazit, E. Self-Assembly of Cyclic Dipeptides: Platforms for Functional Materials. *Protein & Peptide Letters* **2020**, *27*, 688–697. https://doi.org/10.2174/0929866527666200212123542.
7. Zhao, K.; Xing, R.; Yan, X. Cyclic Dipeptides: Biological Activities and Self-assembled Materials. *Peptide Science* **2021**, *113*. https://doi.org/10.1002/pep2.24202.
8. Tao, K.; Fan, Z.; Sun, L.; Makam, P.; Tian, Z.; Ruegsegger, M.; Shaham-Niv, S.; Hansford, D.; Aizen, R.; Pan, Z.; et al. Quantum Confined Peptide Assemblies with Tunable Visible to Near-Infrared Spectral Range. *Nature Communications* **2018**, *9*, 3217. https://doi.org/10.1038/s41467-018-05568-9.
9. Jeziorna, A.; Stopczyk, K.; Skorupska, E.; Luberda-Durnas, K.; Oszajca, M.; Lasocha, W.; Górecki, M.; Frelek, J.; Potrzebowski, M.J. Cyclic Dipeptides as Building Units of Nano- and Microdevices: Synthesis, Properties, and Structural Studies. *Crystal Growth & Design* **2015**, *15*, 5138–5148. https://doi.org/10.1021/acs.cgd.5b01121.
10. Basavalingappa, V.; Bera, S.; Xue, B.; O'Donnell, J.; Guerin, S.; Cazade, P.A.; Yuan, H.; ul Haq, E.; Silien, C.; Tao, K.; et al. Diphenylalanine-Derivative Peptide Assemblies with Increased Aromaticity Exhibit Metal-like Rigidity and High Piezoelectricity. *ACS Nano* **2020**, *14*, 7025–7037. https://doi.org/10.1021/acsnano.0c01654.
11. Tao, K.; Xue, B.; Li, Q.; Hu, W.; Shimon, L.J.; Makam, P.; Si, M.; Yan, X.; Zhang, M.; Cao, Y.; et al. Stable and Optoelectronic Dipeptide Assemblies for Power Harvesting. *Materials Today* **2019**, *30*, 10–16. https://doi.org/10.1016/j.mattod.2019.04.002.
12. Zhao, L.; Yan, X. Supramolecular Self-Assembly: A Facile Way to Fabricate Protein and Peptide Nanomaterials. In *Artificial Protein and Peptide Nanofibers*; Elsevier, 2020; pp. 3–21. https://doi.org/10.1016/B978-0-08-102850-6.00001-2.
13. Tao, K.; Hu, W.; Xue, B.; Chovan, D.; Brown, N.; Shimon, L.J.W.; Maraba, O.; Cao, Y.; Tofail, S.A.M.; Thompson, D.; et al. Bioinspired Stable and Photoluminescent Assemblies for Power Generation. *Advanced Materials* **2019**, *31*, 1807481. https://doi.org/10.1002/adma.201807481.
14. Azuri, I.; Adler-Abramovich, L.; Gazit, E.; Hod, O.; Kronik, L. Why Are Diphenylalanine-Based Peptide Nanostructures so Rigid? Insights from First Principles Calculations. *Journal of the American Chemical Society* **2014**, *136*, 963–969. https://doi.org/10.1021/ja408713x.
15. Tao, K.; Makam, P.; Aizen, R.; Gazit, E. Self-Assembling Peptide Semiconductors. *Science* **2017**, *358*, eaam9756. https://doi.org/10.1126/science.aam9756.
16. Santos, D.; Baptista, R.M.F.; Handa, A.; Almeida, B.; Rodrigues, P.V.; Torres, A.R.; Machado, A.; Belsley, M.; de Matos Gomes, E. Bioinspired Cyclic Dipeptide Functionalized Nanofibers for Thermal Sensing and Energy Harvesting. *Materials* **2023**, *16*, 2477. https://doi.org/10.3390/ma16062477.
17. Haider, A.; Haider, S.; Kang, I.K. A Comprehensive Review Summarizing the Effect of Electrospinning Parameters and Potential Applications of Nanofibers in Biomedical and Biotechnology. *Arabian Journal of Chemistry* **2018**, *11*, 1165–1188. https://doi.org/10.1016/j.arabjc.2015.11.015.
18. Pillay, V.; Dott, C.; Choonara, Y.E.; Tyagi, C.; Tomar, L.; Kumar, P.; du Toit, L.C.; Ndesendo, V.M.K. A Review of the Effect of Processing Variables on the Fabrication of Electrospun Nanofibers for Drug Delivery Applications. *Journal of Nanomaterials* **2013**, *2013*, 1–22. https://doi.org/10.1155/2013/789289.
19. Stoller, P.; Reiser, K.M.; Celliers, P.M.; Rubenchik, A.M. Polarization-Modulated Second Harmonic Generation in Collagen. *Biophysical Journal* **2002**, *82*, 3330–3342. https://doi.org/10.1016/S0006-3495(02)75673-7.
20. Handelman, A.; Shalev, G.; Rosenman, G. Symmetry of Bioinspired Short Peptide Nanostructures and Their Basic Physical Properties. *Israel Journal of Chemistry* **2015**, *55*, 637–644. https://doi.org/10.1002/ijch.201400164.
21. Khanra, S.; Ghosh, K.; Ferreira, F.F.; Alves, W.A.; Punzo, F.; Yu, P.; Guha, S. Probing Nonlinear Optical Coefficients in Self-Assembled Peptide Nanotubes. *Physical Chemistry Chemical Physics* **2017**, *19*, 3084–3093. https://doi.org/10.1039/C6CP07879F.
22. Briscoe, J.; Dunn, S. Piezoelectric Nanogenerators – a Review of Nanostructured Piezoelectric Energy Harvesters. *Nano Energy* **2015**, *14*, 15–29. https://doi.org/10.1016/j.nanoen.2014.11.059.
23. Viezbicke, B.D.; Patel, S.; Davis, B.E.; Birnie, D.P. Evaluation of the Tauc Method for Optical Absorption Edge Determination: ZnO Thin Films as a Model System: Tauc Method for Optical Absorption Edge Determination. *physica status solidi (b)* **2015**, *252*, 1700–1710. https://doi.org/10.1002/pssb.201552007.
24. Zanatta, A.R. Revisiting the Optical Bandgap of Semiconductors and the Proposal of a Unified Methodology to Its Determination. *Scientific Reports* **2019**, *9*, 11225. https://doi.org/10.1038/s41598-019-47670-y.

25. Baptista, R.M.F.; Gomes, C.S.B.; Silva, B.; Oliveira, J.; Almeida, B.; Castro, C.; Rodrigues, P.V.; Machado, A.; Freitas, R.B.; Rodrigues, M.J.L.F.; et al. A Polymorph of Dipeptide Halide Glycyl-L-Alanine Hydroiodide Monohydrate: Crystal Structure, Optical Second Harmonic Generation, Piezoelectricity and Pyroelectricity. *Materials* **2023**, *16*, 3690. https://doi.org/10.3390/ma16103690.
26. You, Y.; Xing, R.; Zou, Q.; Shi, F.; Yan, X. High-Tolerance Crystalline Hydrogels Formed from Self-Assembling Cyclic Dipeptide. *Beilstein Journal of Nanotechnology* **2019**, *10*, 1894–1901. https://doi.org/10.3762/bjnano.10.184.
27. Macha, P.; Perreault, L.; Hamedani, Y.; Mayes, M.L.; Vasudev, M.C. Molecular Mechanisms of Tryptophan–Tyrosine Nanostructures Formation and Their Influence on PC-12 Cells. *ACS Applied Bio Materials* **2018**, *1*, 1266–1275. https://doi.org/10.1021/acsabm.8b00121.
28. Baptista, R.M.F.; de Matos Gomes, E.; Raposo, M.M.M.; Costa, S.P.G.; Lopes, P.E.; Almeida, B.; Belsley, M.S. Self-Assembly of Dipeptide Boc-diphenylalanine Nanotubes inside Electrospun Polymeric Fibers with Strong Piezoelectric Response. *Nanoscale Advances* **2019**, *1*, 4339–4346. https://doi.org/10.1039/C9NA00464E.
29. Costa, J.C.; Taveira, R.J.; Lima, C.F.; Mendes, A.; Santos, L.M. Optical Band Gaps of Organic Semiconductor Materials. *Optical Materials* **2016**, *58*, 51–60. https://doi.org/10.1016/j.optmat.2016.03.041.
30. Baptista, R.M.F.; Silva, B.; Oliveira, J.; Isfahani, V.B.; Almeida, B.; Pereira, M.R.; Cerca, N.; Castro, C.; Rodrigues, P.V.; Machado, A.; et al. High Piezoelectric Output Voltage from Blue Fluorescent N,N-Dimethyl-4-nitroaniline Nano Crystals in Poly-L-Lactic Acid Electrospun Fibers. *Materials* **2022**, *15*, 7958. https://doi.org/10.3390/ma15227958.
31. Baptista, R.M.F.; Moreira, G.; Silva, B.; Oliveira, J.; Almeida, B.; Castro, C.; Rodrigues, P.V.; Machado, A.; Belsley, M.; de Matos Gomes, E. Lead-Free MDABCO-NH4I3 Perovskite Crystals Embedded in Electrospun Nanofibers. *Materials* **2022**, *15*, 8397. https://doi.org/10.3390/ma15238397.
32. Maciel, M.; Ribeiro, S.; Ribeiro, C.; Francesko, A.; Maceiras, A.; Vilas, J.; Lanceros-Méndez, S. Relation between Fiber Orientation and Mechanical Properties of Nano-Engineered Poly(Vinylidene Fluoride) Electrospun Composite Fiber Mats. *Composites Part B: Engineering* **2018**, *139*, 146–154. https://doi.org/10.1016/j.compositesb.2017.11.065.
33. Dias, J.R.; Sousa, A.; Augusto, A.; Bártolo, P.J.; Granja, P.L. Electrospun Polycaprolactone (PCL) Degradation: An In Vitro and In Vivo Study. *Polymers* **2022**, *14*, 3397. https://doi.org/10.3390/polym14163397.
34. Gautam, S.; Chou, C.F.; Dinda, A.K.; Potdar, P.D.; Mishra, N.C. Fabrication and Characterization of PCL/Gelatin/Chitosan Ternary Nanofibrous Composite Scaffold for Tissue Engineering Applications. *Journal of Materials Science* **2014**, *49*, 1076–1089. https://doi.org/10.1007/s10853-013-7785-8.
35. Haifeng Wang.; Weiner, A. Efficiency of Short-Pulse Type-i Second-Harmonic Generation with Simultaneous Spatial Walk-off, Temporal Walk-off, and Pump Depletion. *IEEE Journal of Quantum Electronics* **2003**, *39*, 1600–1618. https://doi.org/10.1109/JQE.2003.819531.
36. Smith, A.V. *Crystal Nonlinear Optics: With SNLO Examples*, 2nd edition ed.; AS-Photonics: Albuquerque, NM, 2018.
37. Baptista, R.M.F.; Lopes, P.E.; Rodrigues, A.R.O.; Cerca, N.; Belsley, M.S.; de Matos Gomes, E. Self-Assembly of Boc- *p* -Nitro- L -Phenylalanyl- *p* -Nitro- L -Phenylalanine and Boc- L -Phenylalanyl- L -Tyrosine in Solution and into Piezoelectric Electrospun Fibers. *Materials Advances* **2022**, *3*, 2934–2944. https://doi.org/10.1039/D1MA01022K.
38. Li, Q.; Jia, Y.; Dai, L.; Yang, Y.; Li, J. Controlled Rod Nanostructured Assembly of Diphenylalanine and Their Optical Waveguide Properties. *ACS Nano* **2015**, *9*, 2689–2695. https://doi.org/10.1021/acsnano.5b00623.
39. Pompa-Monroy, D.A.; Figueroa-Marchant, P.G.; Dastager, S.G.; Thorat, M.N.; Iglesias, A.L.; Miranda-Soto, V.; Pérez-González, G.L.; Villarreal-Gómez, L.J. Bacterial Biofilm Formation Using PCL/Curcumin Electrospun Fibers and Its Potential Use for Biotechnological Applications. *Materials* **2020**, *13*, 5556. https://doi.org/10.3390/ma13235556.